Journal of Molecular Liquids 422 (2025) 127166

Contents lists available at ScienceDirect

Journal of Molecular Liquids

journal homepage: www.elsevier.com/locate/molliq

Exploring macro- and microscopic features of binary L-menthol/xylenol isomers mixtures: An integrated experimental and computational investigation

Ahmad Alhadid [a,1,2], Emanuela Mangiacapre [b,1], Christoforos Tsimopoulos [a], Fabrizio Lo Celso [c], Olga Russina [b], Mirjana Minceva [a,*], Alessandro Triolo [d,*]

[a] Biothermodynamics, TUM School of Life Sciences, Technical University of Munich, Germany
[b] Department of Chemistry, University of Rome Sapienza, Rome, Italy
[c] Department of Physics and Chemistry, University of Palermo, Palermo, Italy
[d] Istituto Struttura della Materia (ISM), Consiglio Nazionale delle Ricerche (CNR), Rome, Italy

ARTICLE INFO

Keywords:
Density
Viscosity
Molecular dynamics simulation
COSMO-RS
Deep eutectic solvents

ABSTRACT

The complex nature of hydrogen bonding interactions in cyclohexyl-phenolic alcohols mixtures motivates investigations of their distinctive characteristics. To this end, we explored macroscopic bulk properties and microscopic features of four binary eutectic mixtures formed by mixing each of the four 2,n-dimethyl phenol (xylenol) isomers (n = 3, 4, 5, 6) and (1R,2S,5R)-2-Isopropyl-5-methylcyclohexanol (L-menthol). The density and viscosity of the mixtures were measured over a wide temperature and composition range. It was found that 2,n-xylenol isomers are denser than L-menthol, and the density of the mixtures decreased with increasing L-menthol mole fraction. L-menthol/2,3-xylenol showed the highest density among the studied mixtures. The larger density of L-menthol/2,3-xylenol was attributed to the negative excess molar volume. On the other hand, 2,n-xylenol isomers are less viscous than L-menthol, and the viscosity of the mixture increased with increasing L-menthol mole fraction. The viscosity of L-menthol/2,3-xylenol, L-menthol/2,4-xylenol, and L-menthol/2,5-xylenol was very similar, while L-menthol/2,6-xylenol showed significantly lower viscosity. This experimental work was complemented with molecular dynamics (MD) simulations on all mixtures with an L-menthol mole fraction of 0.6. The atomistic insight into intermolecular structural correlations provided by MD simulations allows for extracting useful information on the nature of close-neighbor interactions. Analysis of MD simulations allows for highlighting the role of hydrogen bonding interactions and dispersive ones (including aromatic effects) on driving local organization and suggesting potential structural explanations for the experimental observations.

1. Introduction

The growing interest in employing eutectic mixtures as solvents, commonly called deep eutectic solvents (DES), has motivated a surge in both experimental and theoretical research into their physicochemical properties [1]. Eutectic systems are composed of two or more components that are miscible in the liquid phase and crystallize into separate, immiscible solid phases of their constituents [2]. The melting temperature of eutectic mixtures over a certain composition range is lower than that of individual constituents, particularly near the eutectic point [3]. Eutectic systems can be formed by a large pool of substances, including simple organic molecular compounds or salts [4–7]. Accordingly, a variety of eutectic solvents with tunable physicochemical properties were reported in the literature. These eutectic solvents were found superior to conventional organic solvents in various applications such as waste valorization and treatment [8–11], carbon capture [12–14], chemical synthesis and separation [15–17], and extraction of bioactive compounds [18,19].

Beyond the extensive applications of eutectic solvents, the formation of eutectic mixtures offers an opportunity to investigate liquid phase

* Corresponding authors.
E-mail addresses: mirjana.minceva@tum.de (M. Minceva), triolo@ism.cnr.it (A. Triolo).
[1] A. Alhadid and E. Mangiacapre have contributed equally to this work and share first authorship.
[2] Present address: College of Engineering and Technology, American University of the Middle East, Kuwait.

https://doi.org/10.1016/j.molliq.2025.127166
Received 12 October 2024; Received in revised form 12 February 2025; Accepted 14 February 2025
Available online 16 February 2025

properties – such as density and viscosity – at temperatures below the melting points of their neat components. This allows for the exploration of the constituents' supercooled liquid properties, which would otherwise be inaccessible, for instance, due to their high melting temperature or thermal instability. Furthermore, assessing liquid phase properties might provide insights into the unique characteristics of eutectic solvents in the liquid phase.

One of the most widely studied eutectic solvent constituents is L-menthol. L-menthol is a natural terpene that was shown to induce a significant negative deviation from ideality when mixed with phenolic alcohols, such as thymol [20–22], phenol [23], or dimethylphenol (xylenol) isomers [24]. L-menthol/phenolic alcohol mixtures showed a complex solid–liquid equilibrium (SLE) phase diagram, despite being formed from simple organic substances. Moreover, the viscosity of these eutectic systems was significantly higher than that of other L-menthol-based eutectic systems [25,26]. The main feature of the L-menthol/phenolic alcohol eutectic systems is the strong hydrogen bonding interactions between L-menthol (cyclohexyl alcohol) and phenolic alcohols [20]. Nevertheless, the macroscopic properties of their mixtures, such as viscosity, SLE phase diagram, and cocrystal formation, differed for different phenolic alcohol isomers [22,24,25]. Therefore, more detailed investigations of the difference in hydrogen bonding interactions between L-menthol and phenolic alcohol isomers are needed to understand the differences in the macroscopic features of these mixtures. To this end, the synergy between experimental characterization and computational rationalization turns out to be a very successful approach.

In this work, we performed experimental and computational investigations to comprehend the macro- and microscopic features of four eutectic systems, namely, L-menthol/2,3-xylenol (MX_23), L-menthol/2,4-xylenol (MX_24), L-menthol/2,5-xylenol (MX_25), and L-menthol/2,6-xylenol (MX_26). The density and viscosity of the studied eutectic systems were measured over the temperature range 293.1–323.1 K and the composition range in which the mixture is liquid at room temperature. Molecular dynamic simulations were performed on mixtures with L-menthol mole fraction of 0.600 and 303 K, to provide atomistic insight into the structural correlations between L-menthol and the different xylenol isomers. The role of hydrogen bonding and dispersive interactions in driving the local organization and potentially affecting density and viscosity were explored, illustrating the differences due to the different methyl group locations in the 2,n-xylenol isomers. Overall, this study illustrates the power of synergic experimental and computational approaches in highlighting small differences in chemical-physical features in technologically relevant eutectic mixtures.

2. Materials & methods

2.1. Sample preparation

Table 1 shows the chemicals used to prepare the eutectic mixtures, along with their purity and source. All chemicals were used as received without further purification. To ease the handling of samples, the composition of the eutectic systems was selected to cover the composition range where they maintain liquid at room temperature. The SLE phase diagram of MX_23, MX_25, and MX_26 is available in the literature and was used to determine the composition range of prepared mixtures [24]. In contrast, the phase diagram of MX_24 is unavailable in the literature. However, COSMO-RS was reliable in predicting SLE in binary eutectic L-menthol and xylenol isomers systems [24]. Thus, the SLE phase diagram of MX_24 was predicted using COSMO-RS, and the results can be found in Fig. S1 in Electronic Supporting Information (ESI). Details about COSMO-RS calculations can be found in ESI.

Table 1
Chemicals used to prepare the eutectic mixtures.

Name	Purity*	Supplier
L-Menthol	>99 %	Sigma Aldrich
2,3-xylenol	>99 %	Sigma Aldrich
2,4-xylenol	>99 %	Sigma Aldrich
2,5-xylenol	>99 %	Acros Organics
2,6-xylenol	>99 %	Acros Organics

* Determined by GC.

The eutectic mixtures were prepared by mixing L-menthol with the xylenol isomer in prespecified weights (precision 0.1 mg, Sartorius, Germany) inside a tightly sealed vial at 320 K until the liquid appeared clear and homogenous. The samples were filtered using a 0.22 μm PTFE syringe filter and degassed in an ultrasonic bath at 320 K for 5 min. The water content of selected samples was measured using a Coulometric Karl-Fischer Titrator (Hannah Instruments, USA), and the results can be found in Table S2 in ESI.

2.2. Density and viscosity measurements

The density of the eutectic mixtures and pure 2,4-xylenol was measured using a vibrating-tube Densimeter (DMA 4100 M, Anton Paar, Austria). The density was measured over the temperature range 293.1–323.1 K with a 5 K increment, and the composition range in which the mixture is liquid at room temperature.

The viscosity of the eutectic mixtures and pure 2,4-xylenol was measured using a Rheometer (MCR502, Anton Paar, Austria) equipped with a 25 mm cone-plate geometry. The viscosity was measured at a variable shear rate from 1–100 s^{-1} to ensure that the sample showed Newtonian behavior. The reported viscosity was determined at a constant shear rate of 10 s^{-1}, and the value is an average of five measuring points. The viscosity was measured over the temperature range 293.1–328.1 K with a 5 K increment, and the composition range in which the mixture is liquid at room temperature.

Of the five studied substances (see Table 1), only 2,4-xylenol is liquid at room temperature. The density and viscosity of pure 2,4-xylenol in the temperature range 298.1–323.1 K were measured in this work, and density data agreed well with those available in the literature (see Table S3 in ESI).

The molar volume (v) of pure 2,n-xylenol and eutectic systems was calculated as follows

$$v = \frac{M}{\rho} \tag{1}$$

where M is the molecular weight and ρ is the density. The excess molar volume (v^E) was calculated as follows

$$v^E = v^{mix} - \left(\sum x_i v_i^{pure}\right) \tag{2}$$

where v^{mix} is the mixture molar volume; x_i is the mole fraction of component i in the liquid mixture; v_i^{pure} is the molar volume of component i. The deviation from the viscosity of the ideal liquid mixture (Δ_η) was calculated as follows

$$\Delta_\eta = \ln\eta^{mix} - \left(\sum x_i \ln\eta_i^{pure}\right) \tag{3}$$

where η^{mix} is the mixture viscosity and η_i^{pure} is the viscosity of component i.

2.3. Computational details

The molecular structures of the studied components are shown in Fig. 1. Molecular dynamics (MD) simulations were performed using the GROMACS 2021.3 package [27,28]. Bonded and non-bonded parameters for the four systems, L-menthol and its mixture with 2,n-xylenol were described using an all-atoms potential OPLS-AA force field (force field parameters are included in ESI) [29].

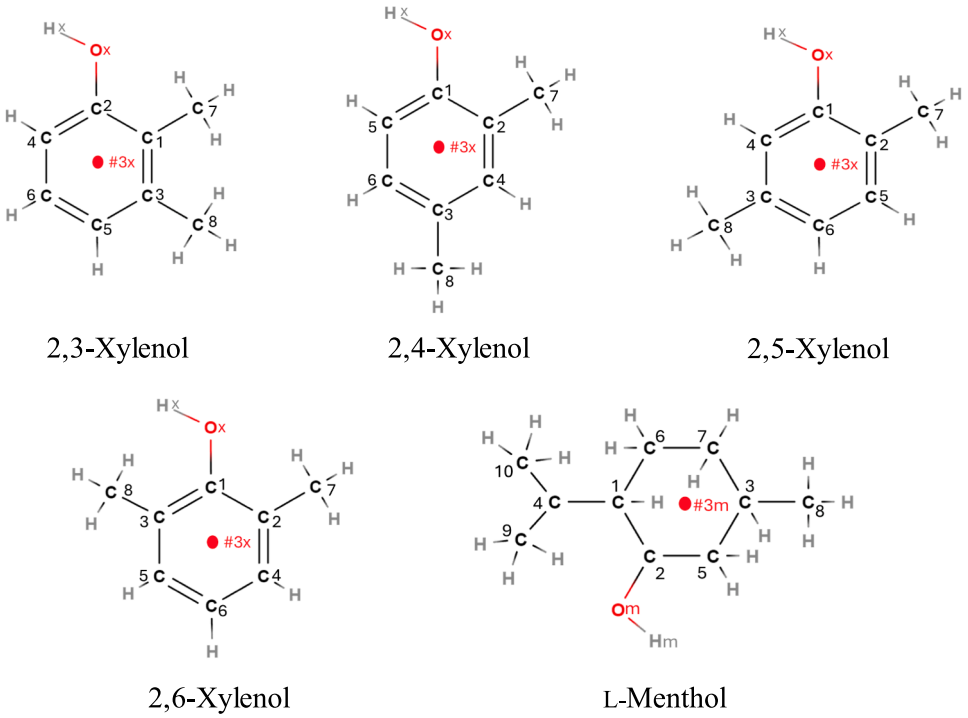

Fig. 1. Molecular structure of studied compounds.

The simulations were performed using a cubic box containing 600 molecules of L-menthol and 400 molecules of 2,n-xylenol to describe mixtures with L-menthol mole fraction of 0.600; periodic boundary conditions were applied. Force field parameter files were created by LigParGen webserver [30–32]; initial configurations were created by Packmol software [33]. Initially, the density was fixed at 10 % lower than the experimental one and progressively converged toward its equilibrium value. The equilibration procedure was done in several steps, starting from a 2 ns NVT simulation at 400 K, followed by a series of 2 ns NPT runs, lowering progressively the temperature to 300 K at 1 bar. After the equilibration phase, the system was run for a total of 100 ns for a production run, and then a trajectory of 2 ns was saved at a frequency of 1 ps for the calculation of the structural properties. The simulations were always checked versus the experimental density and the energy profile. During the production runs for the temperature coupling, we used a velocity-rescaling thermostat [34] (with a time coupling constant of 0.1 ps), while for the pressure coupling, we used a Parrinello–Rahman barostat [35] (1 ps for the relaxation constant). The Leap-Frog algorithm with a 1.0 fs time step was used for integrating the equations of motion. Cut-offs for the Lennard-Jones and real space part of the Coulombic interactions were set to 16 Å. For the electrostatic interactions, the Particle Mesh Ewald (PME) summation method [36,37] was used, with an interpolation order of 6 and 0.08 nm of FFT grid spacing.

X-ray- and neutron-weighted structure factors were computed together with selected pair correlation functions, angular distribution functions, and spatial distribution functions using TRAVIS [38–40]. In the analysis, a virtual atom, indicated as #3 in Fig. 1, has been identified as a geometrical center of rings for each molecular species. Moreover, in our analysis, we also considered the vectors connecting neighbor #3 sites and the vectors perpendicular either to the ring plane for aromatic species or to the plane defined by C atoms in positions 2, 4, and 6 in the aliphatic ring for L-menthol.

3. Results & discussion

3.1. Density of L-menthol/2,n-xylenol mixtures

The density of the mixtures was measured over the temperature range 293.1–323.1 K and the composition range in which the mixture is liquid at room temperature. The results are reported in Tables S4–S7 in ESI. Nevertheless, due to the large amount of data and the need to facilitate the discussion, the density data of samples at a selected temperature and L-menthol mole fraction are discussed. The L-menthol mole fraction near the systems' eutectic point ($x_{menthol}$ = 0.600) and 303.1 K as a temperature were selected. Fig. 2 shows the density of MX_23, MX_24, MX_25, and MX_26 at $x_{menthol}$ = 0.600 as a function of temperature (Fig. 2a) and at 303.1 K as a function of the system composition (Fig. 2b). As seen in Fig. 2a, the density of the eutectic systems is in the order MX_23 > MX_24 = MX_26 > MX_25. Moreover, the density of MX_23 is considerably higher than the other systems, and the temperature dependency of the density of the eutectic mixtures is similar. As seen in Fig. 2b, the density of the eutectic systems at 303.1 K decreases as the mole fraction of L-menthol in the system increases. The density of mixtures depends on the density of pure constituents and their mole fraction in the solution. The density of pure L-menthol is lower compared to 2,n-xylenol isomers due to the more efficient packing of benzene rings compared to cyclohexyl rings [41]. Thus, the density of the eutectic systems decreases due to the lower density of L-menthol compared to 2,n-xylenol isomers [42]. The density order is consistent with that observed in Fig. 2a, and the difference in the density of different systems decreases as the mole fraction of L-menthol in the system increases. The density of pure 2,3-, 2,5-, and 2,6-xylenol is unavailable in the literature due to their higher melting temperatures compared to 2,4-xylenol. Thus, it is not possible to conclude if the density of the eutectic systems is related to the difference in the density of pure 2,n-xylenol isomers.

Assessing the excess molar volume of the systems provides valuable insights into the interactions between the components in the liquid phase. The molar volume of neat 2,3-, 2,5-, and 2,6-xylenol is unavailable in the literature. Hence, we used COSMO-RS to estimate the liquid

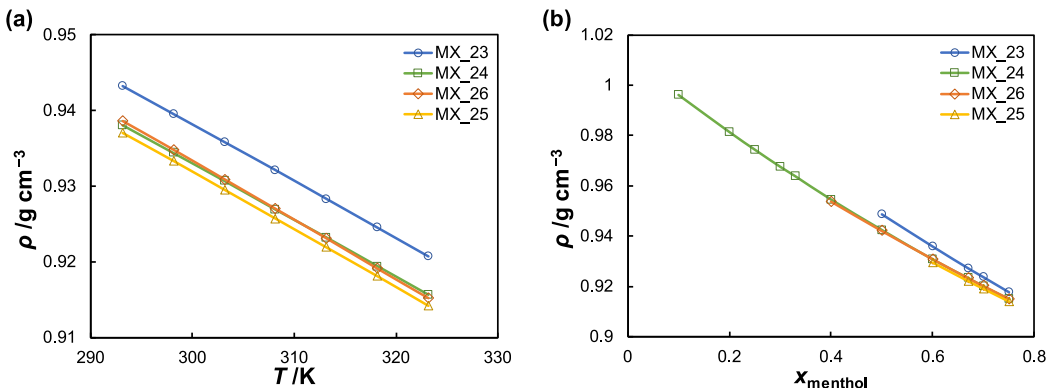

Fig. 2. Density of eutectic mixtures containing L-menthol with 2,3-xylenol (MX_23), 2,4-xylenol (MX_24), 2,5-xylenol (MX_25), and 2,6-xylenol (MX_26) at (a) $x_{\text{menthol}} = 0.600$ and (b) $T = 303.1$ K.

molar volume of pure liquid 2,n-xylenol isomers. Details about COSMO-RS calculations are available in ESI. At first, the COSMO-RS predictions were assessed by comparing experimental and calculated 2,4-xylenol density data, and the results are shown in Fig. S2 in ESI. It was found that COSMO-RS overestimated the molar volume of pure 2,4-xylenol. However, good qualitative predictions were obtained, and a linear correlation between the experimental and calculated molar volume was used to correct the estimated liquid molar volume of pure 2,n-xylenol isomers. The linear correlations and the calculated liquid molar volume of pure 2,n-xylenol are available in Table S8 in ESI. COSMO-RS predicted the following order of the liquid molar volume of pure 2,n-xylenol: 2,6-xylenol > 2,4-xylenol ≈ 2,5-xylenol > 2,3-xylenol. Interestingly, COSMO-RS predicted that 2,3-xylenol has the lowest liquid molar volume among 2,n-xylenol isomers, which is consistent with the density data of the eutectic systems. Thus, the higher density of MX_23 compared to other eutectic systems could be attributed to the higher density of pure liquid 2,3-xylenol.

The estimated liquid molar volume of pure 2,n-xylenol using COSMO-RS–corrected using the linear correlations–was used to estimate the excess molar volume of the eutectic systems at the measured temperature and composition ranges, and the results are shown in Fig. S3 in ESI. The experimental density data of L-menthol available in the literature were used to estimate its pure liquid molar volume. Fig. 3 shows the excess molar volume of the eutectic systems at $x_{menthol} = 0.600$ as a function of temperature (Fig. 3a) and at 303.1 K as a function of the system composition (Fig. 3b). As seen in Fig. 3a, a significant negative excess molar volume is observed in MX_23, which is consistent with the significant negative deviation from ideality observed in the SLE phase diagram of MX_23 [24]. The strong hydrogen bonding interactions between L-menthol and 2,3-xylenol resulted in negative excess molar volume [43]. In contrast, MX_25 shows a slight positive excess molar volume in the temperature range below 308.1 K despite the significant negative deviation from ideal behavior observed in the SLE phase diagram of the system [24]. As seen in Fig. 3b, the system has almost constant excess molar volume over the studied composition range. Thus, MX_25 is considered an ideal mixture based on the mixture molar volume, and the positive excess molar volume is attributed to overestimating the liquid molar volume of pure 2,5-xylenol using COSMO-RS. The observed ideal mixing viscosity in MX_25 might be attributed to the similar position of the methyl groups in 2,5-xylenol and the isopropyl and methyl groups in L-menthol [44].

On the other hand, MX_24 and MX_26 show a negative excess molar volume at 303.1 K over the studied composition range. Despite the near-ideal behavior observed in the SLE phase diagram of the system [24], MX_26 shows a larger negative excess molar volume than MX_24. However, the excess molar volume value in MX_26 might be overestimated due to COSMO-RS underestimating the liquid molar volume of pure 2,6-xylenol. As seen in Fig. 3b, the excess molar volume of MX_26 at 303.1 K shows a minimum value at the eutectic composition of the system ($x_{menthol} \approx 0.550$), while the minimum value of excess molar volume in MX_23 and MX_24 is not observed at the systems' eutectic composition.

In conclusion, assessing the excess molar volume of the studied L-menthol/2,n-xylenol isomers systems indicates that the excess molar volume is not related to the deviation from ideal behavior observed in the SLE phase diagram of the systems. MX_23 shows the largest excess

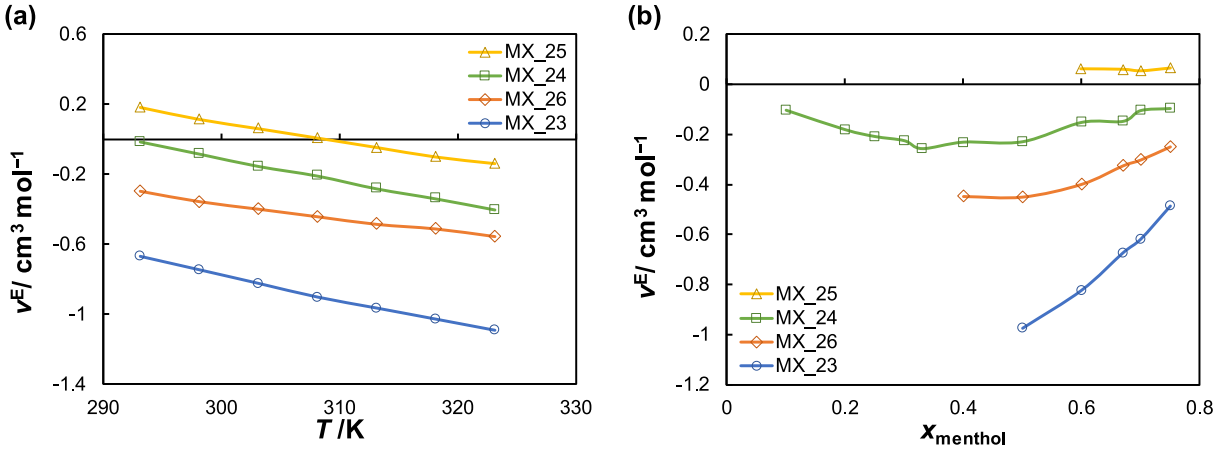

Fig. 3. Excess volume in eutectic mixtures containing L-menthol with 2,3-xylenol (MX_23), 2,4-xylenol (MX_24), 2,5-xylenol (MX_25), and 2,6-xylenol (MX_26) at (a) $x_{\text{menthol}} = 0.600$ and (b) $T = 303.1$ K.

molar volume, which correlates with the higher density of MX_23 among the studied systems.

3.2. Viscosity of L-menthol/2,n-xylenol mixtures

The viscosity of MX_23, MX_24, MX_25, and MX_26 at the temperature range 293.1–328.1 K and the composition range in which the mixture is liquid at room temperature was measured, and the results are reported in Tables S9–S12. Fig. 4 shows the viscosity of MX_23, MX_24, MX_25, and MX_26 at $x_{menthol} = 0.600$ as a function of temperature (Fig. 4a) and at 303.1 K as a function of the system composition (Fig. 4b). As seen in Fig. 4a, the viscosity of MX_23, MX_24, and MX25 is similar and significantly higher than MX_26, and the difference is more considerable at lower temperatures. As seen in Fig. 4b, the viscosity of the studied systems increases when the mole fraction of L-menthol in the mixture increases. The increase in the mixture viscosity when increasing the L-menthol mole fraction is attributed to the higher viscosity of L-menthol compared to phenolic alcohols [25].

The viscosity of eutectic mixtures depends on the viscosity of pure constituents. Assessing the deviation from the ideal mixing viscosity provides insight into the intermolecular interaction in the liquid solution and aids in modeling the viscosity of eutectic mixtures [26,45]. Only the viscosity of pure 2,4-xylenol was measured in this work, while the viscosity of 2,3-, 2,5-, and 2,6-xylenol was estimated using COSMO-RS. Details about COSMO-RS calculations can be found in ESI. COSMO-RS predictions of the viscosity of pure 2,n-xylenol isomers are assessed by comparing experimental and calculated viscosity of pure 2,4-xylenol (see Fig. S4 in ESI). It was found that COSMO-RS underestimated the viscosity of pure 2,4-xylenol isomer, particularly at low temperatures. Hence, a quadratic correlation between the experimental and calculated viscosity was used to correct the estimated viscosity of pure 2,n-xylenol, and the results can be found in Table S13 in ESI. COSMO-RS predicted that 2,4-xylenol has the highest viscosity, which is similar to that of 2,3-xylenol. On the other hand, the predicted viscosity of 2,6-xylenol is significantly lower than the other 2,n-xylenol isomers. Thus, COSMO-RS predictions for the viscosity of pure 2,n-xylenol isomers are consistent with the measured viscosity of the L-menthol/2,n-xylenol isomers systems, as evident from the significantly lower viscosity of MX_26 compared to the other studied eutectic systems.

Next, the estimated viscosity of 2,n-xylenol isomers from COSMO-RS and those calculated for L-menthol using the Vogel-Fulcher-Tammann (VFT) equation [26] were used to calculate the deviation from the ideal mixing viscosity of the studied systems, and the results are shown in Fig. S5 in ESI. Fig. 5 shows the deviation from the viscosity of the ideal liquid mixture of the eutectic systems at $x_{menthol} = 0.600$ as a function of temperature (Fig. 5a) and at 303.1 K as a function of the system composition (Fig. 5b). As seen in Fig. 5a, a negative deviation from the ideal mixing viscosity is observed in all systems at low temperatures, indicating that the actual viscosity of the eutectic mixture is lower than the ideal mixing viscosity. The deviation from the ideal mixing viscosity decreases at higher temperatures, indicating that the negative deviation from the ideal mixing viscosity could be attributed to the uncertainty of extrapolating the viscosity of pure L-menthol using the VFT model [26]. Nevertheless, at high temperatures, where experimental data of L-menthol viscosity are available, a positive deviation from the ideal mixing viscosity is observed in MX_23, while a negative deviation from the ideal mixing viscosity is observed in MX_26. On the other hand, at temperatures higher than 313.1 K, near-ideal mixing viscosity is observed for MX_24 and MX_25. As seen in Fig. 5b, the negative deviation from the ideal mixing viscosity increases as the L-menthol mole fraction in the mixture increases, which further confirms that the negative deviation from the ideal mixing viscosity is attributed to the uncertainty of extrapolating the viscosity of L-menthol to lower temperatures. To rule out the uncertainty of extrapolating the viscosity of L-menthol, the deviation from the ideal mixing viscosity was analyzed at 323.1 K (see Fig. S5). It was found that the maximum deviation from the ideal mixing viscosity is near the eutectic point in all studied systems except for MX_26. Moreover, the largest deviation from the ideal mixing viscosity is observed in MX_23. Thus, the intermolecular interactions might influence the deviation from ideal mixing viscosity, as shown in previous studies [25,46]. Unlike the molar volume, the viscosity of the L-menthol/2,n-xylenol isomers systems seems to be correlated with the negative deviation from ideality.

3.3. Intermolecular correlations and structural features

Computed density values obtained from MD simulations at 300 K and $x_{menthol} = 0.600$ for all the simulated mixtures are in very good agreement with experimentally determined density, with a maximum deviation of 1.6 % observed in MX_26. The comparison between experimental and MD-calculated density values is presented in Table S14 of the ESI. Fig. S6 shows the X-ray weighted static structure factors (S(q)) that were determined computationally via MD simulations for all studied systems.

Computed S(q) data for the MX_2n series are quite similar, showing no significant differences. Specifically, S(q) patterns reveal a sharp peak at approximately 1.2 $Å^{-1}$ (corresponding to a Bragg size $d = 2\pi/q = 5.3$ Å) with a shoulder at around 0.6 $Å^{-1}$ (corresponding to $d = 2\pi/q = 10.5$ Å). The former feature indicates the presence of close neighbor molecules in the liquid state, while the latter is characteristic of amorphous compounds such as ionic glasses and "fragile" glass-forming liquids

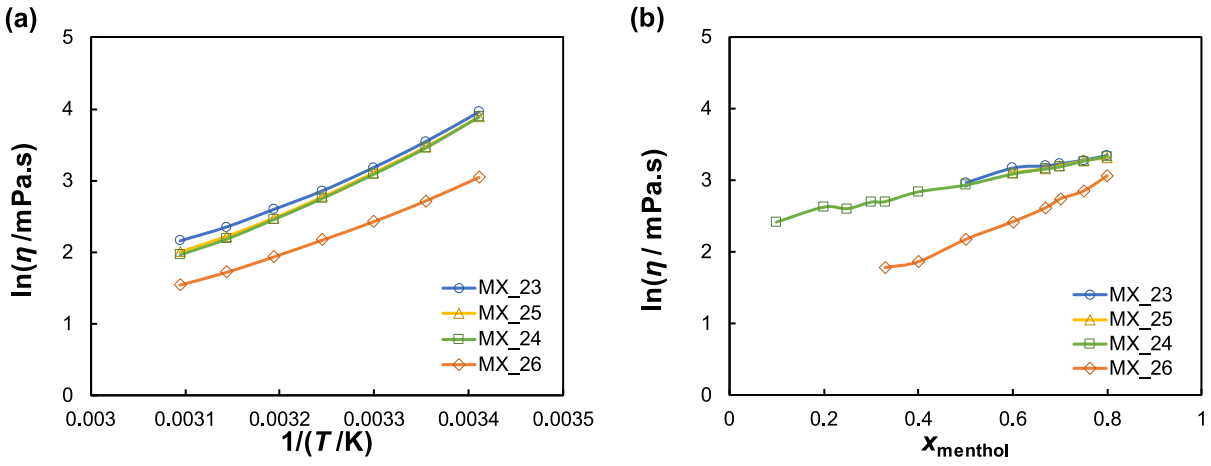

Fig. 4. Viscosity of eutectic mixtures containing L-menthol with 2,3-xylenol (MX_23), 2,4-xylenol (MX_24), 2,5-xylenol (MX_25), and 2,6-xylenol (MX_26) at (a) $x_{menthol} = 0.600$ and (b) $T = 303.1$ K.

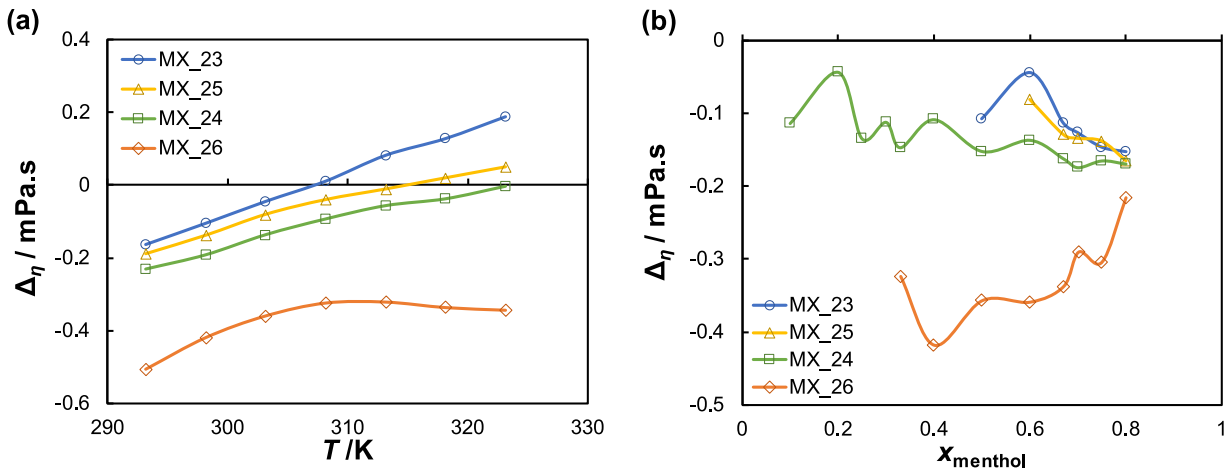

Fig. 5. Deviation from the ideal mixing viscosity in eutectic mixtures containing L-menthol with 2,3-xylenol (MX_23), 2,4-xylenol (MX_24), 2,5-xylenol (MX_25), and 2,6-xylenol (MX_26) at (a) $x_{menthol} = 0.600$ and (b) $T = 303.15$ K.

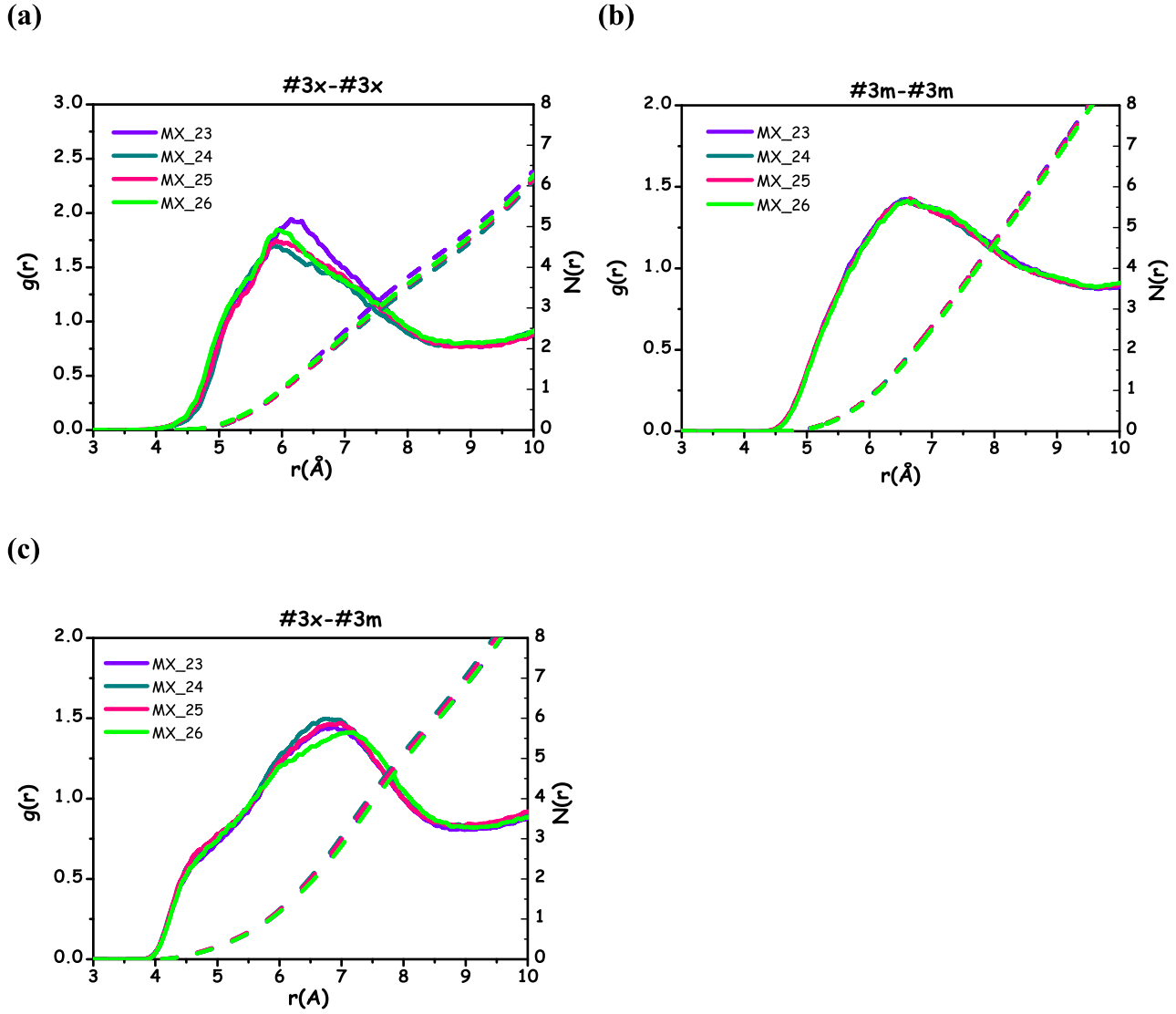

Fig. 6. MD-computed rdfs (continuous lines) and the corresponding running neighbor numbers (dashed lines) related to #3x_#3x (a), #3m-#3m (b) and #3x-#3m (c) correlations for the MX_2n systems.

[47,48]. These features are also observed in many DESs [49–54], pure liquids such as carvacrol and molten thymol [55] and ionic liquids [56–59]. In particular, low-q peaks suggest a *meso*-scale organization, with small hydrogen-bonded clusters embedded in an aromatic/aliphatic matrix formed by L-menthol and/or xylenol rings for all the probed systems.

Neutron-weighted static structure factors in the case of either no deuteration, selective deuteration of one or the other, or both, species (Fig. S7) are also computed. Therein, no remarkable differences were observed among the neutron-weighted data for all the cases explored, except for a feature at approximately 3 $Å^{-1}$ in the MX_23 system with deuterated L-menthol, which shows a higher amplitude than corresponding features for the other mixtures (see Fig. S7).

To gain further structural information, Fig. S8 depicts the neutron-weighted simulated S(q) obtained by selectively deuterating only hydroxyl groups of both L-menthol and xylenol. Interestingly, the characteristic peaks at approximately 0.6 $Å^{-1}$ and 1.2 $Å^{-1}$ appear as two distinct features when n = 3, 4, and 5. On the other hand, for n = 6, the peak at around 0.6 $Å^{-1}$ merges with the main peak at 1.2 $Å^{-1}$, similar to the MD-computed X-ray weighted static structure factor.

By analysing the neutron-weighted S(q) patterns with either no or –OH deuteration (in Fig. S7 and Fig. S8, respectively), it appears that the merging of these peaks, for n = 6, is mostly due to the shift of the peak at 0.6 $Å^{-1}$ to higher values, approximately 0.7 $Å^{-1}$.

This suggests that the presence of the methyl group at n = 6 hinders the formation of well-structured H-bonded clusters involving L-menthol and xylenol hydroxyl groups. This phenomenon might explain the notably lower viscosity observed in the MX_26 mixture as compared with the other mixtures. The lack of well-structured H-bonded clusters and aggregates likely reduces the system's resistance to flow, resulting in lower measured viscosity.

In Fig. 6, we report the radial distribution functions (rdfs or g(r)s) between M or X ring centers (RC, #3) in the different MX_2n systems.

Considering xylenol-xylenol RC (#3x-#3x) correlations (Fig. 6a), we observe a sharp peak with a large amplitude, centered at approximately 6 Å, with about five nearest neighbors for each mixture when integrated up to a distance of 9 Å. This peak appears quite structured, as it appears as a combination of different peaks centered at around 5 Å, 6 Å, and 7.5 Å. Regarding the L-menthol-L-menthol RC (#3m-#3m) correlations (Fig. 6b), only a broad peak is detected, whose shape, amplitude,

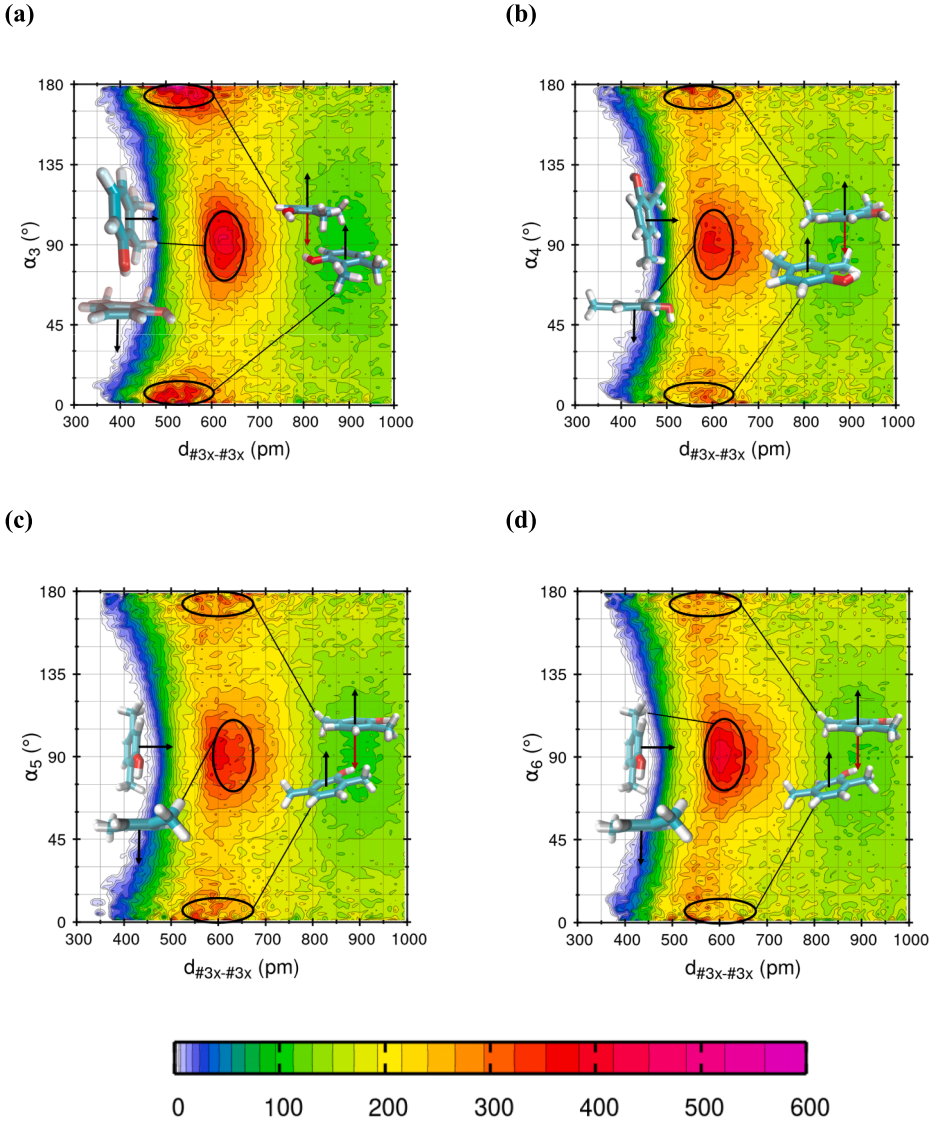

Fig. 7. MD-computed combined distribution functions (cdfs) for the #3x-#3x correlation where the angle between the vectors perpendicular to the center of neighbor rings (α_n where n = 3, 4, 5, and 6 based on the xylenol methylation) are observed as a function of centers distance $d_{\#3x\text{-}\#3x}$ for (a) MX_23, (b) MX_24, (c) MX_25, and (d) MX_26.

position, and corresponding number of neighbors remain essentially unaffected by the position of the methyl group in the xylenol molecule, reaching a value of about 6 considering a distance of 9 Å. Lastly, xylenol-L-menthol RC (#3x-#3m) correlations are characterized by the merging of three peaks centered at approximately 5 Å, 6 Å and 7.6 Å, with minor changes upon modifying the xylenol isomer and numbers of coordination equal to 6 (Fig. 6c).

A better understanding of these correlations can be achieved using the combined distribution functions (cdfs). Specifically, Fig. 7 presents cdfs related to the mutual orientation of the rings as a function of their distance in each MX_2n system. From Fig. 7, it is evident that a strong perpendicular orientation between neighbor xylenol rings occurs at a distance of approximately 6 Å. However, at a shorter distance of around 5 Å, both parallel ($\alpha_n \approx 0°$) and antiparallel ($\alpha_n \approx 180°$) orientations are observed, as well, although these latter orientations are favored for n = 3 and particularly disfavoured for n = 6. This specific behavior for n = 6 might be a reason for the relatively low viscosity observed. The corresponding cdf for the case of L-menthol-L-menthol correlations is shown in Fig. S9 in the ESI. It appears that the pseudo-parallel alignment of rings (L-menthol is not planar) at a distance of approximately 7 Å is lost. This result can be related to the lack of π-aromatic electron density in L-menthol, which leads to a non-planar geometry. Moreover, at distances ranging from 5 Å to 7 Å, a structured antiparallel ($150° < \beta_n < 180°$) organization with three main lobes is observed.

Fig. S10 shows cdfs concerning the correlations related to the possible xylenol and L-menthol rings interactions for all the MX_2n systems. It is evident that all explored cases exhibit parallel ($\gamma_n \approx 0°$) and antiparallel ($\gamma_n \approx 180°$) ring orientations at distances between 4 Å and 5 Å. At larger distances (approximately 7 Å), perpendicular orientations are also detected. No clear differences are observed between these cdfs when the position of the methyl group in the xylenol is varied. Overall, these results indicate that the presence of the aromatic ring induces an extended range correlation, with a parallel alignment of the ring, for molecules separated as much as 7 Å. L-menthol-L-menthol correlations do not extend to such a large distance, as only weak parallel alignment was found.

Due to the aromatic nature of the xylenol molecule, we also considered the possibility of the existence of π-π interactions between the rings. Fig. 8 presents the cdf related to the angle between the vector #3x-#3x and the one perpendicular to the observed ring as a function of

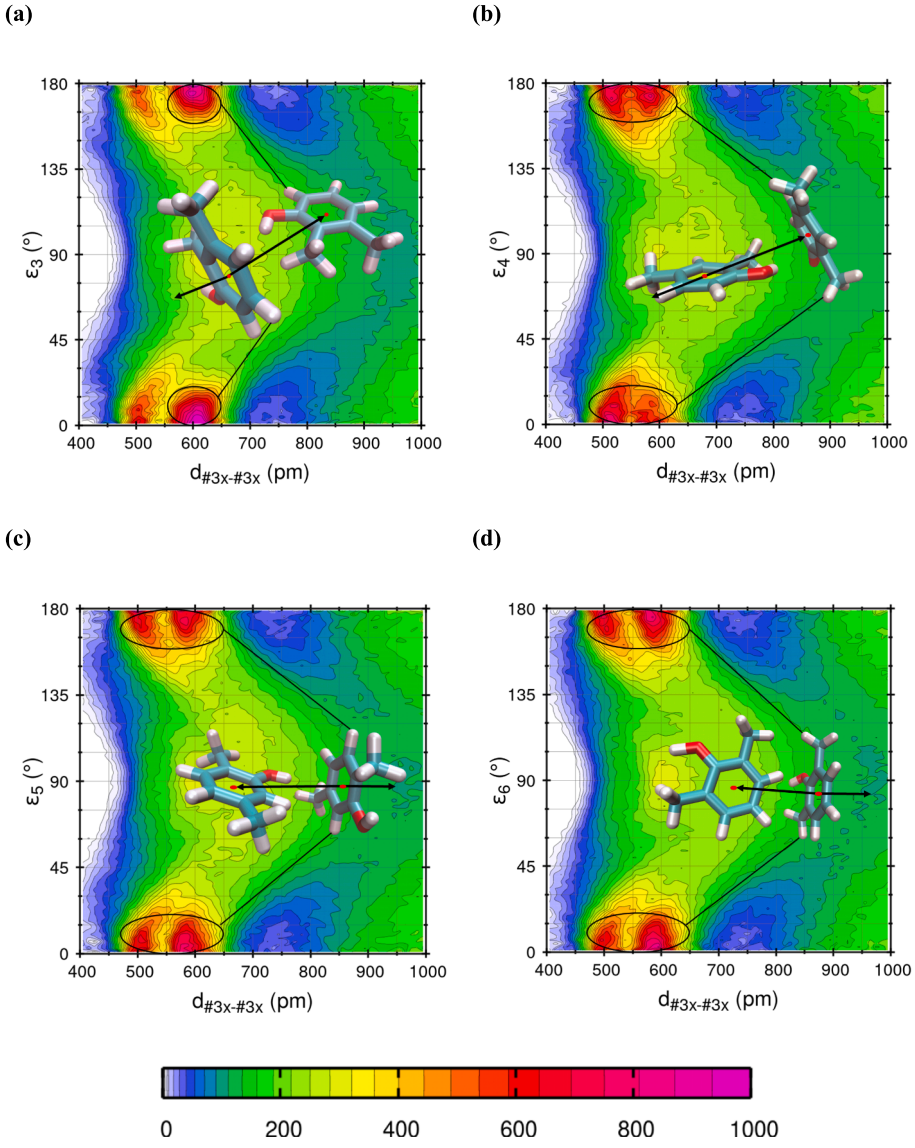

Fig. 8. MD-computed combined distribution functions (cdfs) for the #3x-#3x correlation where angles between the vectors parallel to d#3x-#3x and the vectors perpendicular to the center of the rings (εn where n = 3,4,5, and 6 based on the xylenol methylation) are observed as a function of centers distance d#3x-#3x for all the MX_2n systems.

$d_{\#3x\text{-}\#3x}$. It emerges that all the probed systems exhibit two main features centered at 5 Å and 6 Å, where we observe parallel ($\varepsilon_n \approx 0$–$15°$) and antiparallel ($\varepsilon_n \approx 165$–$180°$) arrangements of the mentioned vectors. The spot centered at approximately 6 Å is more intense for the system with n = 3. However, in all the cases examined, the comparison between Figs. 7 and 8 suggest that no stacked π-π interactions (that would correspond to values of $\varepsilon_n \approx 90°$) are detectable, although parallel rings can be found, with a shifted location of neighbor rings.

Further structural analysis involves exploring hydrogen bonding interactions between xylenol and L-menthol hydroxyl groups (Fig. 9). Considering xylenol as the Hydrogen Bond Acceptor (HBA) species, as shown in Fig. 9a and b, we observe a relatively strong interaction with both xylenol and L-menthol Hydrogen Bond Donor (HBD) species, respectively, characterized by a peak centered at approximately 2.0 Å. Integrating this feature for the Ox-Hx and Ox-Hm correlations up to a distance of 2.7–2.8 Å, we find that Ox engages in hydrogen bonding interactions with approximately 0.20 Hm and 0.15–0.18 Hx, with slight variations depending on the position of the second methyl group in xylenol. These coordination numbers result in an average of approximately 0.35 hydrogen atoms interacting with Ox.

Similarly, considering L-menthol as the HBA species, for the Om-Hm correlation (Fig. 9c), we observe a peak centered at approximately 2.0 Å. However, this feature exhibits a high intensity, reaching a value of almost 6. A similar observation can be made for the Om-Hx correlation (Fig. 9d), where a very intense peak centered at approximately 2.0 Å is detected. Considering L-menthol as HBA, Om has a total coordination number ranging between 0.71–0.77 for both Hx and Hm in all the explored cases. A detailed description of the number of nearest neighbors related to the different hydrogen bonding interactions is provided in Table S15 in ESI.

Additionally, Om-Hm correlations appear unaffected by the methyl group position in xylenol molecules, analogously to #3m-#3m correlations. An intensity ranking related to the population of the HB population is observed, particularly for the Ox-Hx, Ox-Hm, and Om-Hx correlations. Table 2 shows the observed intensity scales for each investigated correlation in Fig. 9.

It is evident that the strongest hydrogen bonding interactions occur in systems with either n = 3 or n = 4. Additionally, in all explored cases, the hydrogen bonding interactions in MX_26 are the weakest in the series. As an example, Fig. S11 reports the cdf related to the Ox-Hm interaction, thus considering L-menthol and xylenol as HBD and HBA species, respectively.

It is evident that in all the probed systems, there are very strong hydrogen bonding interactions between the hydroxyl groups of L-menthol and xylenol, with the former acting as the donor and the latter as the acceptor. Specifically, each interaction is characterized by a hot spot centered at approximately 2.0 Å with an angular range between 0 and 15°. Additionally, the representative snapshots corresponding to

Table 2
Number of HB interactions obtained from the rdfs related to HBs between hydroxyl groups of L-menthol and xylenol molecules in MX_2n systems.

Correlation	Number of HB interactions
Ox-Hx	MX_23 > MX_24 > MX_25 > MX_26
Ox-Hm	MX_24 = MX_25 > MX_23 > MX_26
Om-Hm	MX_23 = MX_24 = MX_25 = MX_26
Om-Hx	MX_24 > MX_23 > MX_25 > MX_26

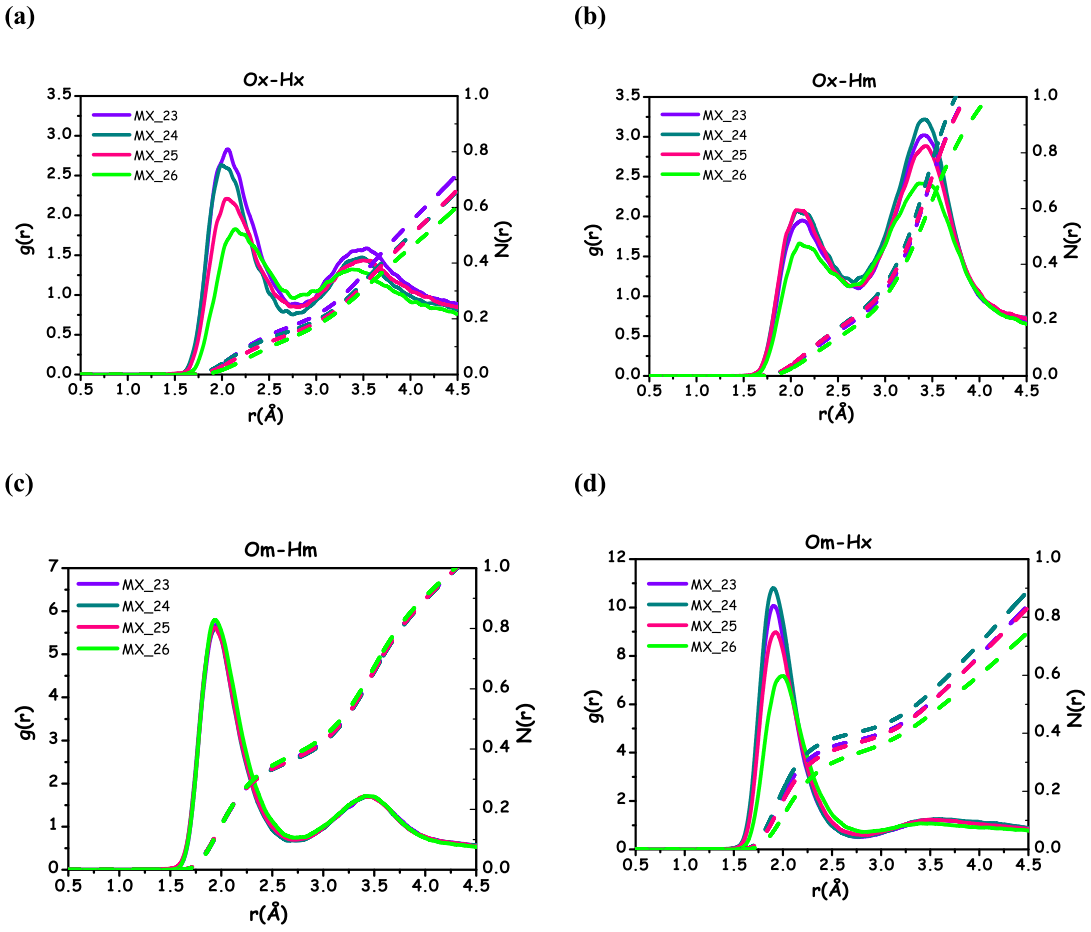

Fig. 9. MD-computed rdfs (continuous lines) and corresponding running neighbor numbers (dashed lines) for the Ox-Hx (a), Ox-Hm (b), Om-Hm (c) and Om-Hx (d) correlations.

the hot spots show that in each system, L-menthol and xylenol tend to structurally organize one above the other due to the strong HB interaction. Such a situation might explain the difficulty encountered by the aromatic species to face each other and engage in π-π stacking, as shown above in Fig. 8. Indeed, L-menthol tends to engage in HB interactions with xylenol, hindering the location above/below the aromatic ring. This observation aligns with the findings in Fig. 6, showing that xylenol and L-menthol rings are positioned closer to each other compared to xylenol rings among themselves.

We also explored the possibility of both L-menthol and xylenol hydroxyl groups engaging in O-H···π interactions with the xylenol ring, a non-conventional HB already observed in pure aromatic liquids [55] and in different mixtures composed of an aromatic species and a non-aromatic molecule [50,60]. Specifically, Fig. S12 shows the #3x-Hx (a) and #3x-Hm (b) correlations for all the examined mixtures.

It is evident that in both explored cases, the presence of π···H–O interactions does not depend on the position of xylenol methylation. Specifically, for the #3x-Hx correlation, we can observe a first peak centered at approximately 2.8 Å, with a coordination number of around 0.2. On the other hand, for the #3x-Hm correlation, a sharper peak is clearly evident, centered at approximately 2.6 Å, with a coordination number of about 0.5.

To deepen these observations, we explore the effect of local π···H–O interactions for all the MX_2n systems using the cdfs. Specifically, in Fig. S13 in ESI we show the cdfs related to the #3x-Hx correlation where the angle between the vectors perpendicular to the rings is described as a function of $d_{Hx\text{-}\#3x}$. It is evident that in all cases, there is a hot spot centered around 3 Å where the rings tend to position themselves perpendicularly to each other ($75^\circ < \theta_n < 105^\circ$).

In the MX_23 system, the simultaneous presence of strong hydrogen bonding interactions between hydroxyl groups and relatively intense π···H–O interactions could explain the significant deviation from ideal behavior when mixing L-menthol and 2,3-xylenol. These strong intermolecular interactions in MX_23 align with the measured SLE phase diagram [24], the negative excess molar volume, and the positive deviation from the ideal mixing viscosity observed in this study.

Finally, we also show the strong tendency of L-menthol hydroxyl hydrogen to be engaged in π···H–O interactions with the xylenol ring for all the MX_2n systems (Fig. S14). In all cases, no significant differences were detected based on xylenol methylation; moreover, xylenol and L-menthol rings show a clear tendency to arrange themselves in parallel ($\delta_n \approx 0^\circ$) and antiparallel ($\delta_n \approx 180^\circ$) orientations at a distance of 3 Å. It is noteworthy to mention that such an HB correlation is characterized by different ring orientations in the case of xylenol or L-menthol acting as HBD. The former tends to organize in a perpendicular way to the acceptor ring, while the latter tends to lay parallel while developing the π···H–O interaction.

4. Conclusion

This work presents a comprehensive experimental and computational analysis for four binary eutectic systems formed by mixing L-menthol with 2,3-, 2,4-, 2,5-, and 2,6-xylenol isomers, highlighting the differences in chemical-physical features in these technologically relevant eutectic mixtures.

The density and viscosity of the eutectic systems were measured at different temperatures and compositions. It was found that 2,n-xylenol isomers are denser than L-menthol, and the density of the mixtures decreased with increasing L-menthol mole fraction. MX_23 showed the highest density among the studied mixtures, while MX_24 and MX_26 possess similar densities. In contrast, MX_25 showed the lowest density. The larger density of MX_23 was attributed to the negative excess molar volume, while the lower density of MX_25 resulted from the slightly positive excess molar volume. On the other hand, 2,n-xylenol isomers are less viscous than L-menthol, and the viscosity of the mixture increased with increasing the L-menthol mole fraction. The viscosity of MX_23, MX_24, and MX_25 was very similar, while MX_26 showed significantly lower viscosity. MX_23 showed a positive deviation from the ideal mixing viscosity, while a negative deviation from the ideal mixing viscosity was observed in MX_26. In contrast, the viscosity of MX_24 and MX_25 did not deviate from the ideal mixing viscosity.

MD simulations described the nature of microscopic interactions between L-menthol and the different xylenol, providing atomistic insight into correlations responsible for macroscopic features. The principal interaction driving the local morphology in MX mixtures is hydrogen bonding, and MD shows that L-menthol is the main actor as HB acceptor species, with minimal differences due to the location of the methyl group position in the different xylenol isomers. Interactions between hydroxyl groups (either from M or from X molecules) and the center of X rings, which are associated with the establishment of π···H–O interactions, have been detected. These interactions lead to a perpendicular arrangement between neighbor xylenols or to a parallel arrangement when L-menthol is the donor species. In MX_23, the concomitancy of strong hydrogen bonding interactions between hydroxyl groups and relatively intense π···H–O interactions could help in rationalizing the significant deviation from ideal behavior in this mixture, as reflected by the SLE phase diagram [24], the negative excess molar volume, and the positive deviation from the viscosity of the ideal liquid mixture observed in this study. Dispersive interactions also drive the structural organization in the L-menthol/2,n-xylenol isomers mixtures. We detect privileged parallel orientation between neighbor pairs involving aromatic species, while neighbor pairs involving L-menthol tend to organize in a parallel/antiparallel way. In any case, the present study does not detect the formation of π··π stacks between neighbor xylenols, presumably due to the intrusion of strongly hydrogen-bonded L-menthol molecules close to xylenols.

Overall, this study comprehensively describes the experimental physicochemical properties and local structure correlations at a microscopic level on an interesting example of cyclohexyl and phenolic alcohol mixtures, which are presently gaining much attention as “deep” eutectic solvents.

CRediT authorship contribution statement

Ahmad Alhadid: Writing – original draft, Supervision, Methodology, Investigation, Formal analysis, Data curation, Conceptualization. **Emanuela Mangiacapre:** Writing – original draft, Investigation, Formal analysis, Data curation. **Christoforos Tsimopoulos:** Investigation, Formal analysis, Data curation. **Fabrizio Lo Celso:** Investigation. **Olga Russina:** Writing – original draft, Investigation, Data curation. **Mirjana Minceva:** Writing – review & editing, Supervision, Conceptualization. **Alessandro Triolo:** Writing – original draft, Investigation, Formal analysis, Data curation.

Declaration of competing interest

The authors declare that they have no known competing financial interests or personal relationships that could have appeared to influence the work reported in this paper.

Acknowledgments

This work has been partly supported by European Union – Next Generation EU in the framework of the PRIN 2022 SEED4GREEN – Code 20223W4RT9.

AT acknowledges support by the project ECS00000024 “Ecosistemi dell’Innovazione” - Rome Technopole of the Italian Ministry of University and Research, public call n. 3277, PNRR - Mission 4, Component 2, Investment 1.5, financed by the European Union, Next Generation EU.

OR and EM were supported by the University of Rome Sapienza Projects: “Green solvents for simple and complex carbohydrates” (RM120172B2165468) and “Hydrophilic vs hydrophobic eutectic

solvents for oligosaccharides." (RM12218152014836).

Appendix A. Supplementary data

Supplementary data to this article can be found online at https://doi.org/10.1016/j.molliq.2025.127166.

Data availability

Data supporting the work findings are available in the manuscript and Supplementary Material file.

References

[1] A.T.H. Yeow, A. Hayyan, M. Hayyan, M. Usman Mohd Junaidi, J. Saleh, W. Jefrey Basirun, M. Roslan Mohd Nor, W. Al Abdulmonem, M. Zulhaziman, M. Salleh, F. Mohamed Zuki, M. Diana Hamid, A comprehensive review on the physicochemical properties of deep eutectic solvents, Results Chem. 7 (2024) 101378, https://doi.org/10.1016/j.rechem.2024.101378.

[2] Gamsjäger, H., W. Lorimer John, P. Scharlin, and G. Shaw David, *Glossary of terms related to solubility (IUPAC Recommendations 2008)*, in *Pure Appl. Chem.* 2008. p. 233.

[3] A. van den Bruinhorst, M. Costa Gomes, Is there depth to eutectic solvents? Curr. Opin. Green Sustainable Chem. 37 (2022) 100659 https://doi.org/10.1016/j.cogsc.2022.100659.

[4] D.J.G.P. van Osch, C.H.J.T. Dietz, S.E.E. Warrag, M.C. Kroon, The Curious Case of Hydrophobic Deep Eutectic Solvents: A Story on the Discovery, Design, and Applications, ACS Sustain. Chem. Eng. 8 (29) (2020) 10591–10612, https://doi.org/10.1021/acssuschemeng.0c00559.

[5] D.J.G.P. van Osch, C.H.J.T. Dietz, J. van Spronsen, M.C. Kroon, F. Gallucci, M. van Sint Annaland, R. Tuinier, A Search for Natural Hydrophobic Deep Eutectic Solvents Based on Natural Components, ACS Sustain. Chem. Eng. 7 (3) (2019) 2933–2942, https://doi.org/10.1021/acssuschemeng.8b03520.

[6] A. Khalid, S. Tahir, A.R. Khalid, M.A. Hanif, Q. Abbas, M. Zahid, Breaking new grounds: metal salts based-deep eutectic solvents and their applications- a comprehensive review, Green Chem. 26 (5) (2024) 2421–2453, https://doi.org/10.1039/D3GC04112C.

[7] D.O. Abranches, J.A.P. Coutinho, Type V deep eutectic solvents: Design and applications, Curr. Opin. Green Sustainable Chem. 35 (2022) 100612, https://doi.org/10.1016/j.cogsc.2022.100612.

[8] S. Suffia, D. Dutta, Applications of deep eutectic solvents in metal recovery from E-wastes in a sustainable way, J. Mol. Liq. 394 (2024) 123738, https://doi.org/10.1016/j.molliq.2023.123738.

[9] R.F. González-Laredo, V.I. Sayago-Monreal, M.R. Moreno-Jiménez, N.E. Rocha-Guzmán, J.A. Gallegos-Infante, L.F. Landeros-Macías, M. Rosales-Castro, Natural deep eutectic solvents (NaDES) as an emerging technology for the valorisation of natural products and agro-food residues: a review, Int. J. Food Sci. Technol. 58 (12) (2023) 6660–6673, https://doi.org/10.1111/ijfs.16641.

[10] M.K. Al Hassan, A. Alfarsi, M.S. Nasser, I.A. Hussein, I. Khan, Ionic liquids and NADES for removal of organic pollutants and heavy metals in wastewater: A comprehensive review, J. Mol. Liq. 391 (2023) 123163, https://doi.org/10.1016/j.molliq.2023.123163.

[11] J.F. Grisales-Mejía, V. Cedeño-Fierro, J.P. Ortega, H.G. Torres-Castañeda, M. M. Andrade-Mahecha, H.A. Martínez-Correa, G. Álvarez-Rivera, J.A. Mendiola, A. Cifuentes, E. Ibañez, Advanced NADES-based extraction processes for the recovery of phenolic compounds from Hass avocado residues: A sustainable valorization strategy, Sep. Purif. Technol. 351 (2024) 128104, https://doi.org/10.1016/j.seppur.2024.128104.

[12] Z. Guo, Z. Zhang, Y. Huang, T. Lin, Y. Guo, L.N. He, T. Liu, CO(2) Valorization in Deep Eutectic Solvents, ChemSusChem 17 (18) (2024) e202400197, https://doi.org/10.1002/cssc.202400197.

[13] I. Wazeer, M.K. Hadj-Kali, I.M. Al-Nashef, Utilization of Deep Eutectic Solvents to Reduce the Release of Hazardous Gases to the Atmosphere: A Critical Review, Molecules 26 (1) (2021), https://doi.org/10.3390/molecules26010075.

[14] R. Biswas, Physicochemical Properties and Applications of Deep Eutectic Solvents for CO2 Capture, Chem. Eng. Technol. 47 (1) (2024) 20–35, https://doi.org/10.1002/ceat.202300161.

[15] S. Verma, K. Saini, S. Maken, Deep eutectic solvents: A long–term approach to chemical synthesis and separation, J. Mol. Liq. 393 (2024) 123605, https://doi.org/10.1016/j.molliq.2023.123605.

[16] Y. Elhamarnah, H. Qiblawey, M. Nasser, A review on Deep eutectic solvents as the emerging class of green solvents for membrane fabrication and separations, J. Mol. Liq. 398 (2024) 124250, https://doi.org/10.1016/j.molliq.2024.124250.

[17] A.S. Alqahtani, Indisputable roles of different ionic liquids, deep eutectic solvents and nanomaterials in green chemistry for sustainable organic synthesis, J. Mol. Liq. 399 (2024) 124469, https://doi.org/10.1016/j.molliq.2024.124469.

[18] D. Szopa, P. Wróbel, A. Witek-Krowiak, Enhancing polyphenol extraction efficiency: A systematic review on the optimization strategies with natural deep eutectic solvents, J. Mol. Liq. 404 (2024) 124902, https://doi.org/10.1016/j.molliq.2024.124902.

[19] C.U. Mussagy, H.U. Hucke, N.F. Ramos, H.F. Ribeiro, M.B. Alves, A. Mustafa, J.F. B. Pereira, F.O. Farias, Tailor-made solvents for microbial carotenoids recovery, Appl. Microbiol. Biotechnol. 108 (1) (2024) 234, https://doi.org/10.1007/s00253-024-13049-x.

[20] D.O. Abranches, M.A.R. Martins, L.P. Silva, N. Schaeffer, S.P. Pinho, J.A. P. Coutinho, Phenolic hydrogen bond donors in the formation of non-ionic deep eutectic solvents: the quest for type V DES, Chem. Commun. 55 (69) (2019) 10253–10256, https://doi.org/10.1039/c9cc04846d.

[21] A. Alhadid, C. Jandl, L. Mokrushina, M. Minceva, Experimental Investigation and Modeling of Cocrystal Formation in L-Menthol/Thymol Eutectic System, Cryst. Growth Des. 21 (11) (2021) 6083–6091, https://doi.org/10.1021/acs.cgd.1c00306.

[22] A. Alhadid, L. Mokrushina, M. Minceva, Formation of glassy phases and polymorphism in deep eutectic solvents, J. Mol. Liq. 314 (2020) 113667, https://doi.org/10.1016/j.molliq.2020.113667.

[23] A. Alhadid, C. Jandl, L. Mokrushina, M. Minceva, Cocrystal Formation in l-Menthol/Phenol Eutectic System: Experimental Study and Thermodynamic Modeling, Cryst. Growth Des. 22 (6) (2022) 3973–3980, https://doi.org/10.1021/acs.cgd.2c00362.

[24] A. Alhadid, C. Jandl, L. Mokrushina, M. Minceva, Nonideality and cocrystal formation in l-menthol/xylenol eutectic systems, J. Mol. Liq. 367 (2022) 120582, https://doi.org/10.1016/j.molliq.2022.120582.

[25] A. Alhadid, L. Mokrushina, M. Minceva, Influence of the Molecular Structure of Constituents and Liquid Phase Non-Ideality on the Viscosity of Deep Eutectic Solvents, Molecules 26 (14) (2021), https://doi.org/10.3390/molecules26144208.

[26] D. Peng, A. Alhadid, M. Minceva, Modeling the viscosity of binary eutectic systems at different compositions and temperatures, J. Mol. Liq. 373 (2023) 121258, https://doi.org/10.1016/j.molliq.2023.121258.

[27] B. Hess, C. Kutzner, D. van der Spoel, E. Lindahl, GROMACS 4: Algorithms for Highly Efficient, Load-Balanced, and Scalable Molecular Simulation, J. Chem. Theory Comput. 4 (3) (2008) 435–447, https://doi.org/10.1021/ct700301q.

[28] D. Van Der Spoel, E. Lindahl, B. Hess, G. Groenhof, A.E. Mark, H.J.C. Berendsen, GROMACS: Fast, flexible, and free, J. Comput. Chem. 26 (16) (2005) 1701–1718, https://doi.org/10.1002/jcc.20291.

[29] W.L. Jorgensen, D.S. Maxwell, J. Tirado-Rives, Development and Testing of the OPLS All-Atom Force Field on Conformational Energetics and Properties of Organic Liquids, J. Am. Chem. Soc. 118 (45) (1996) 11225–11236, https://doi.org/10.1021/ja9621760.

[30] L.S. Dodda, I. Cabeza de Vaca, J. Tirado-Rives, W.L. Jorgensen, LigParGen web server: an automatic OPLS-AA parameter generator for organic ligands, Nucleic Acids Res. 45 (W1) (2017) W331–W336, https://doi.org/10.1093/nar/gkx312.

[31] W.L. Jorgensen, J. Tirado-Rives, Potential energy functions for atomic-level simulations of water and organic and biomolecular systems, Proc. Natl. Acad. Sci. 102 (19) (2005) 6665–6670, https://doi.org/10.1073/pnas.0408037102.

[32] L.S. Dodda, J.Z. Vilseck, J. Tirado-Rives, W.L. Jorgensen, 1.14*CM1A-LBCC: Localized Bond-Charge Corrected CM1A Charges for Condensed-Phase Simulations, J. Phys. Chem. B 121 (15) (2017) 3864–3870, https://doi.org/10.1021/acs.jpcb.7b00272.

[33] L. Martínez, R. Andrade, E.G. Birgin, J.M. Martínez, PACKMOL: A package for building initial configurations for molecular dynamics simulations, J. Comput. Chem. 30 (13) (2009) 2157–2164, https://doi.org/10.1002/jcc.21224.

[34] G. Bussi, D. Donadio, M. Parrinello, Canonical sampling through velocity rescaling, J. Chem. Phys. 126 (1) (2007) 014101, https://doi.org/10.1063/1.2408420.

[35] M. Parrinello, A. Rahman, Polymorphic transitions in single crystals: A new molecular dynamics method, J. Appl. Phys. 52 (12) (1981) 7182–7190, https://doi.org/10.1063/1.328693.

[36] T. Darden, D. York, L. Pedersen, Particle mesh Ewald: An N·log(N) method for Ewald sums in large systems, J. Chem. Phys. 98 (12) (1993) 10089–10092, https://doi.org/10.1063/1.464397.

[37] U. Essmann, L. Perera, M.L. Berkowitz, T. Darden, H. Lee, L.G. Pedersen, A smooth particle mesh Ewald method, J. Chem. Phys. 103 (19) (1995) 8577–8593, https://doi.org/10.1063/1.470117.

[38] M. Brehm, B. Kirchner, TRAVIS – A Free Analyzer and Visualizer for Monte Carlo and Molecular Dynamics Trajectories, J. Chem. Inf. Model. 51 (8) (2011) 2007–2023, https://doi.org/10.1021/ci200217w.

[39] O. Hollóczki, M. Macchiagodena, H. Weber, M. Thomas, M. Brehm, A. Stark, O. Russina, A. Triolo, B. Kirchner, Triphilic Ionic-Liquid Mixtures: Fluorinated and Non-fluorinated Aprotic Ionic-Liquid Mixtures, ChemPhysChem 16 (15) (2015) 3325–3333, https://doi.org/10.1002/cphc.201500473.

[40] M. Brehm, M. Thomas, S. Gehrke, B. Kirchner, TRAVIS-A free analyzer for trajectories from molecular simulation, J. Chem. Phys. 152 (16) (2020) 164105, https://doi.org/10.1063/5.0005078.

[41] R.P. Singh, C.P. Sinha, Viscosities and activation energies of viscous flow of the binary mixtures of n-hexane with toluene, chlorobenzene and 1-hexanol, J. Chem. Eng. Data 29 (2) (1984) 132–135, https://doi.org/10.1021/je00036a010.

[42] M.A.R. Martins, E.A. Crespo, P.V.A. Pontes, L.P. Silva, M. Bülow, G.J. Maximo, E.A. C. Batista, C. Held, S.P. Pinho, J.A.P. Coutinho, Tunable Hydrophobic Eutectic Solvents Based on Terpenes and Monocarboxylic Acids, ACS Sustain. Chem. Eng. 6 (7) (2018) 8836–8846, https://doi.org/10.1021/acssuschemeng.8b01203.

[43] S. Verma, A. Sharma, S. Maken, Volumetric, transport and acoustic properties of binary mixtures containing alkanol at 298.15–318.15 K, J. Mol. Liq. 390 (2023) 123029, https://doi.org/10.1016/j.molliq.2023.123029.

[44] S. Verma, M. Rani, H. Song, S. Maken, Studies on thermodynamics properties of binary mixtures of amyl acetate with propanol at T=298.15 K to 318.15 K, J. Mol. Liq. 400 (2024) 124534, https://doi.org/10.1016/j.molliq.2024.124534.

[45] A. Prabhune, A. Mathur, S. Saha, R. Dey, Predictive, correlative and machine learning models for estimation of viscosity of liquid mixtures, J. Mol. Liq. 397 (2024) 124147, https://doi.org/10.1016/j.molliq.2024.124147.

[46] S. Verma, S. Kim, S. Maken, Y. Lee, Thermodynamic and molecular simulation analysis of molecular interactions between methyl 2–hydroxyisobutyrate + water or n–alkanol (C1–C2) mixtures, J. Mol. Liq. 392 (2023) 123461, https://doi.org/10.1016/j.molliq.2023.123461.
[47] S.R. Elliott, The origin of the first sharp diffraction peak in the structure factor of covalent glasses and liquids, J. Phys. Condens. Matter 4 (38) (1992) 7661, https://doi.org/10.1088/0953-8984/4/38/003.
[48] W. Xu, E.I. Cooper, C.A. Angell, Ionic Liquids: Ion Mobilities, Glass Temperatures, and Fragilities, J. Phys. Chem. B 107 (25) (2003) 6170–6178, https://doi.org/10.1021/jp0275894.
[49] N. Schaeffer, D.O. Abranches, L.P. Silva, M.A.R. Martins, P.J. Carvalho, O. Russina, A. Triolo, L. Paccou, Y. Guinet, A. Hedoux, J.A.P. Coutinho, Non-Ideality in Thymol + Menthol Type V Deep Eutectic Solvents, ACS Sustain. Chem. Eng. 9 (5) (2021) 2203–2211, https://doi.org/10.1021/acssuschemeng.0c07874.
[50] A. Triolo, F. Lo Celso, O. Russina, Liquid structure of a water-based, hydrophobic and natural deep eutectic solvent: The case of thymol-water. A Molecular Dynamics study, J. Mol. Liq. 372 (2023) 121151, https://doi.org/10.1016/j.molliq.2022.121151.
[51] A. Malik, H.K. Kashyap, Heterogeneity in hydrophobic deep eutectic solvents: SAXS prepeak and local environments, PCCP 23 (6) (2021) 3915–3924, https://doi.org/10.1039/D0CP05407K.
[52] A. Gupta, H.K. Kashyap, Nanoscale heterogeneity, hydrogen bonding and their temperature dependence in cholinium phenylalaninate bio-ionic liquid, J. Mol. Liq. 326 (2021) 115329, https://doi.org/10.1016/j.molliq.2021.115329.
[53] S. Kaur, A. Gupta, H.K. Kashyap, Nanoscale Spatial Heterogeneity in Deep Eutectic Solvents, J. Phys. Chem. B 120 (27) (2016) 6712–6720, https://doi.org/10.1021/acs.jpcb.6b04187.
[54] A. Malik, H.K. Kashyap, Origin of structural and dynamic heterogeneity in thymol and coumarin-based hydrophobic deep eutectic solvents as revealed by molecular dynamics, PCCP 25 (29) (2023) 19693–19705, https://doi.org/10.1039/D3CP01770B.
[55] E. Mangiacapre, A. Triolo, F. Ramondo, F. Lo Celso, O. Russina, Unveiling the structural organisation of carvacrol through X-ray scattering and molecular Dynamics: A comparative study with liquid thymol, J. Mol. Liq. 394 (2024) 123778, https://doi.org/10.1016/j.molliq.2023.123778.
[56] O. Russina, A. Triolo, L. Gontrani, R. Caminiti, Mesoscopic Structural Heterogeneities in Room-Temperature Ionic Liquids, J. Phys. Chem. Lett. 3 (1) (2012) 27–33, https://doi.org/10.1021/jz201349z.
[57] O. Russina, A. Triolo, New experimental evidence supporting the mesoscopic segregation model in room temperature ionic liquids, Faraday Discuss. 154 (2012) 97–109, https://doi.org/10.1039/C1FD00073J.
[58] A. Triolo, O. Russina, H.-J. Bleif, E. Di Cola, Nanoscale Segregation in Room Temperature Ionic Liquids, J. Phys. Chem. B 111 (18) (2007) 4641–4644, https://doi.org/10.1021/jp067705t.
[59] F. Lo Celso, Y. Yoshida, F. Castiglione, M. Ferro, A. Mele, C.J. Jafta, A. Triolo, O. Russina, Direct experimental observation of mesoscopic fluorous domains in fluorinated room temperature ionic liquids, PCCP 19 (20) (2017) 13101–13110, https://doi.org/10.1039/C7CP01971H.
[60] C. Di Mino, A.G. Seel, A.J. Clancy, T.F. Headen, T. Földes, E. Rosta, A. Sella, N. T. Skipper, Strong structuring arising from weak cooperative O-H···π and C-H···O hydrogen bonding in benzene-methanol solution, Nat. Commun. 14 (1) (2023) 5900, https://doi.org/10.1038/s41467-023-41451-y.